Control of a Powered Ankle–Foot Prosthesis Based on a Neuromuscular Model

Michael F. Eilenberg, Hartmut Geyer, and Hugh Herr, *Member, IEEE*

***Abstract*—Control schemes for powered ankle–foot prostheses rely upon fixed torque–ankle state relationships obtained from measurements of intact humans walking at target speeds and across known terrains. Although effective at their intended gait speed and terrain, these controllers do not allow for adaptation to environmental disturbances such as speed transients and terrain variation. Here we present an adaptive muscle-reflex controller, based on simulation studies, that utilizes an ankle plantar flexor comprising a Hill-type muscle with a positive force feedback reflex. The model's parameters were fitted to match the human ankle's torque-angle profile as obtained from level-ground walking measurements of a weight and height-matched intact subject walking at 1 m/s. Using this single parameter set, clinical trials were conducted with a transtibial amputee walking on level ground, ramp ascent, and ramp descent conditions. During these trials, an adaptation of prosthetic ankle work was observed in response to ground slope variation, in a manner comparable to intact subjects, without the difficulties of explicit terrain sensing. Specifically, the energy provided by the prosthesis was directly correlated to the ground slope angle. This study highlights the importance of neuromuscular controllers for enhancing the adaptiveness of powered prosthetic devices across varied terrain surfaces.**

***Index Terms*—Neuromuscular model, powered prosthesis, prosthesis control, terrain adaptation.**

I. Introduction

TODAY'S commercially-available ankle–foot prostheses utilize lightweight, passive structures that are designed to present appropriate elasticity during the stance phase of walking [1], [2]. The advanced composites used in these devices permit some energy storage during controlled dorsiflexion and plantar flexion, and subsequent energy release during powered plantar flexion, much like the Achilles tendon in the intact human [3], [4]. Although this passive-elastic behavior is a good approximation to the ankle's function during slow walking, normal and fast walking speeds require the addition of external energy, and thus cannot be implemented by any passive ankle–foot device [5]–[7]. This deficiency is reflected in the gait of transtibial amputees using passive ankle–foot prostheses. Their self-selected walking speed is slower, and stride length shorter, than normal [8]. In addition, their gait is distinctly asymmetric: the range of ankle movement on the unaffected side is smaller [9], [10], while, on the affected side, the hip extension moment is greater and the knee flexion moment is smaller [8], [10]. They also expend greater metabolic energy walking than nonamputees [11]–[16]. These differences could possibly be a result of the amputees' greater use of hip power to compensate for the lack of ankle power [17]–[19].

To provide for a normal, economical gait beyond slow walking speeds, powered ankle–foot prostheses have now been developed [20]–[26], [31]. Some of these are of size and weight comparable to the intact human ankle–foot, and have the elastic energy storage, motor power, and battery energy to provide for a day's typical walking activity [31]. The use of active motor power in these prostheses raises the issue of control. In previous work with these powered devices, the approach taken was to match the torque–ankle state profile of the intact human ankle for the activity to be performed [24], [26], [27]. The provision of motor power meant that the open work loops of the angle-torque profiles in faster walking could be supported, rather than just the spring-like behavior provided by passive devices. However, this control approach exhibited no inherent adaptation. Instead, torque profiles were required for all intended activities and variation of terrain, along with an appropriate means to select among them.

In this study, in an attempt to produce a controller with the ability to adapt, we instead evaluate the use of a neuromuscular model with a positive force feedback reflex scheme as the basis of control. Such models have been employed in simulation studies of the biomechanics of legged locomotion [28], [29] and show promise regarding terrain adaptation. The present work applies this type of neuromuscular model as part of the control system for a powered ankle–foot prosthesis. The controller presented here employs a model of the ankle–foot complex for determining the physical torque to command at the ankle joint. In this model, the ankle joint is provided with two virtual actuators. For plantar flexion torque, the actuator is a Hill-type muscle with a positive force feedback reflex scheme. This scheme models the reflexive muscle response due to some combination of afferent signals from muscle spindles and Golgi tendon organs. For dorsiflexion torque, an impedance is provided by a virtual rotary spring-damper.

The parameters of this neuromuscular model were fitted by an optimization procedure to provide the best match between the measured ankle torque of an intact subject walking at a target speed of 1.0 m/s, and the model's output torque when given

Manuscript received February 20, 2009; revised July 07, 2009; accepted July 22, 2009. First published January 12, 2010; current version published April 21, 2010. This work was supported in part by the U.S. Veterans Administration under Grant VA241-P-0026, in part by the Army Telemedicine and Advanced Technology Division under Grant W81XWH-07-1-0343, and in part by an EU Marie Curie Fellowship to Hartmut Geyer (MOIF-CT-20052-022244).

M. Eilenberg is with the Mechanical Engineering Department, Massachusetts Institute of Technology (MIT) and the MIT Media Laboratory, Cambridge, MA 02139 USA (e-mail: emichael@media.mit.edu).

H. Geyer is with the is with the Robotics Institute, Carnegie Mellon University, Pittsburgh, PA 15213 USA (e-mail: hgeyer@cs.cmu.edu).

H. Herr is with the Harvard/Massachusetts Institute of Technology (MIT), Division of Health Sciences and Technology and the MIT Media Laboratory, MIT, Cambridge, MA 02139 USA (e-mail: hherr@media.mit.edu).

Digital Object Identifier 10.1109/TNSRE.2009.2039620

as inputs the measured motion of the intact subject. The neuromuscular model-based prosthetic controller was used to provide torque commands to a powered ankle–foot prosthesis worn by an amputee. This control strategy was evaluated using two criteria. First, the controller was tested for the ability to produce prosthesis ankle torque and ankle angle profiles that qualitatively match those of a comparable, intact subject at a target level-ground walking speed. The second performance criterion was the controller's ability to exhibit a biologically-consistent trend of increasing gait cycle network for increasing walking slope without changing controller parameters. Detecting variations in ground slope is difficult using typical sensors, so a controller with an inherent ability to adapt to these changes is of particular value.

II. Methods

A. Ankle–Foot Prosthesis

The ankle–foot prosthesis used for this study, shown in Fig. 1(a), is one in development by iWalk, LLC. This prosthesis is a successor to the series of prototypes developed in the Biomechatronics Group of the MIT Media Laboratory. It is a completely self contained device having the weight (1.8 kg) and size of the intact biological ankle–foot complex.

1) Mechanical Components: The ankle joint is a rolling bearing design joining a lower foot structure to an upper leg shank structure topped with a prosthetic pyramid fixture for attachment to the amputee's socket. The foot includes a passive low profile Flex-Foot [1] to minimize ground contact shock to the amputee. A unidirectional leaf spring, the *parallel spring*, acts across the ankle joint, engaging when the ankle and foot are perpendicular to each other. It acts in parallel to a powered drive train, providing the passive function of an Achilles tendon. The powered drive train is a motorized link across the ankle joint as represented in Fig. 1(b). From the upper leg shank end, it consists, in series, of a brushless motor, (Powermax EC-30, 200 W, 48 V, Maxon) operating at 24 V, a belt drive transmission with 40/15 reduction, and a 3-mm pitch linear ball screw. At this operating voltage, the theoretical maximum torque that can be generated by the motor through the drivetrain is approximately 340 Nm.

At the foot, the *series spring*, a Kevlar-composite leaf spring, connects the foot to the ball nut with a moment arm, r_s, that is direction-dependent. Therefore, the effective rotary stiffness of the series spring, as evaluated by locking the drive train and exerting a torque about the ankle joint, is 533 N·m/rad for positive torque, and 1200 N·m/rad for negative torque, where positive torque (or plantar flexion torque) is that tending to compress the series spring as represented in Fig. 1(c). The drive train and the series spring together comprise a series-elastic actuator (SEA) [30]. The arrangement of these components is shown schematically in Fig. 1(c).

2) Sensors: A hall-effect angle sensor at the ankle joint is a primary control input, and has a range of -0.19 to 0.19 radians, where zero corresponds to the foot being perpendicular to the shank. Joint angle is estimated with a linear hall-effect sensor (Allegro A1395) mounted on the main housing. This sensor

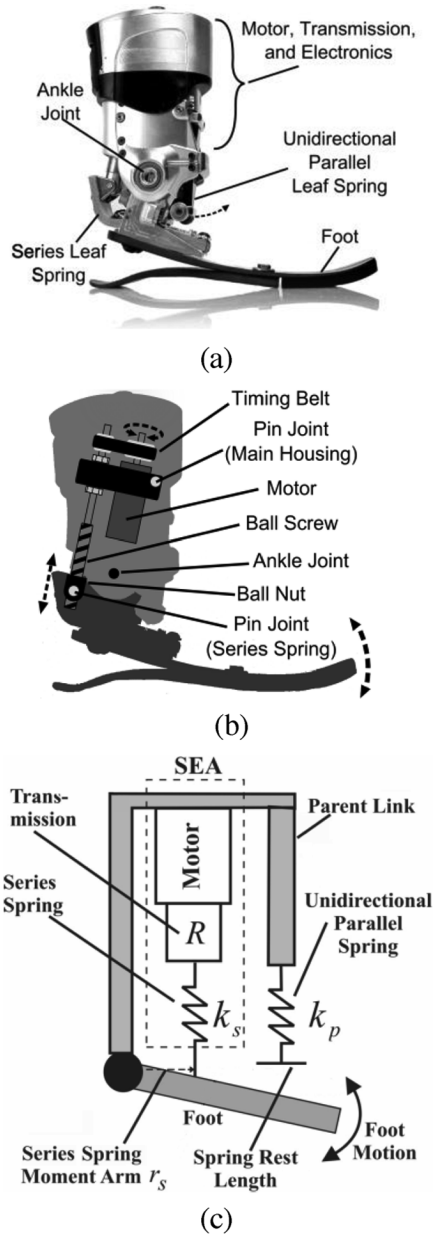

Fig. 1. (a) Physical system with labeled components, (b) diagram of the drive train, and (c) mechanical model of the powered ankle–foot prosthesis. The rotary elements in the photograph are shown as linear equivalents in the model schematic for clarity.

is proximate to a magnet that is rigidly connected to the foot structure so that the magnetic axis is tangent to the arc of the magnet's motion. As a result of this arrangement, the magnetic field strength at the sensor location varies as the magnet rotates past the sensor. Strain gauges are located inside the prosthetic pyramid attachment, allowing for an estimate of the torque at the ankle joint. Strain gauges located on the series spring permit sensing of the output torque of the motorized drive train, thereby allowing for closed-loop force control of the SEA. The motor itself contains Hall-effect commutation sensors and is fitted with an optical shaft encoder that enables the use of advanced brushless motor control techniques.

3) Microcontroller: Overall control and communications for the ankle–foot prosthesis are provided by a single-chip, 16-bit,

DSP oriented microcontroller, the Microchip Technology Incorporated dsPIC33FJ128MC706. The microcontroller operates at 40 million instructions per second, with 128 kB of flash program memory, and 16 384 B of RAM. It provides adequate computation to support real time control.

4) Motor Controller: A second 16-B dsPIC33FJ128MC706 was used as a dedicated motor controller. The high computation load and speed requirements of modern brushless motor control methodologies, along with task isolation from the main microcontroller's real time demands motivated this architecture. A high speed digital link between the main microcontroller and the motor microcontroller supplied virtually instantaneous command of the motor.

5) Wireless Interface: For development and data collection, a high-speed serial port of the microcontroller is dedicated to external communications. This port may be used directly via cable or may have a wide variety of wireless communication devices attached. For the present study, the 500 Hz sensor and internal state information is telemetered over the serial port at 460 Kilobaud and transmitted via an IEEE 802.11g wireless local area network device (Lantronix Wiport).

6) Battery: All power for the prosthesis was provided by a 0.22 kg lithium polymer battery having a 165 Watt-Hour/kg energy density. The battery was able to provide a day's power requirements including 5000 steps of powered walking.

7) Optimal Mechanical Component Selection: Meeting the requirements for mass, size, torque, speed, energy efficiency, shock tolerance, and nearly silent operation is not a trivial task. Of particular importance is the modeling and optimization of the drive train for the production of the biological torques and motions of walking. Some effects of the motor selection, overall transmission ratio, series elastic spring, and parallel spring are described in [31].

B. Control Architecture

The purpose of the control architecture is to command an ankle torque appropriate to the amputee's gait cycle as determined from available sensor measurements of prosthetic ankle state. The controller determines the appropriate torque using a neuromuscular model of the human ankle–foot complex. In this model, a hinge joint, representing the human ankle joint, is actuated by two competing virtual actuators as depicted in Fig. 5(a): a unidirectional plantar flexor which is a Hill-type muscle model, and a dorsiflexor which acts as either a bi-directional proportional-derivative position controller, or a unidirectional virtual rotary spring-damper, depending on the gait phase. A finite state machine maintains an estimate of the phase of the amputee's gait. Depending on this estimated gait phase, one or the other, or both of the virtual actuators produce torques at the virtual ankle joint. The net virtual torque is then used as the ankle torque command to the prosthesis hardware. Physical torque at the ankle joint is produced by both the motorized drive train and the parallel spring. The ankle angle sensor is used to determine the torque produced by the parallel spring, and the remaining desired torque is commanded through the motor controller.

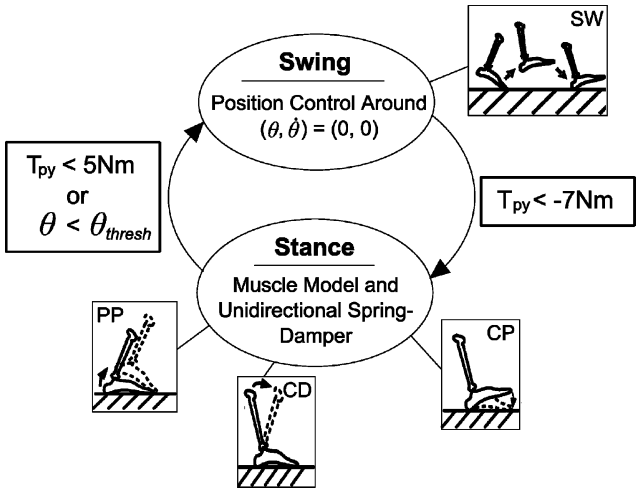

Fig. 2. Finite state machine with state transition thresholds and equivalent ankle–foot biomechanics during each state. Swing is labeled SW, and stance is divided into controlled plantar flexion (CP), controlled dorsiflexion (CD), and powered plantar flexion (PP) as in [5]. State transitions are determined using the prosthesis ankle torque, T_P, as measured from the pyramid strain gauges, and prosthesis ankle angle, θ.

1) Top Level State Machine Control: Top level control of the prosthesis is implemented by a finite state machine synchronized to the gait cycle. During walking, two states are recognized: swing phase and stance phase. Prosthesis sensor inputs (ankle torque as estimated from the pyramid strain gauges, ankle angle, and motor velocity) are continuously observed to determine state transitions. Conditions for these state transitions were experimentally determined. Fig. 2 depicts the operation of the state machine and transition conditions. The dorsiflexor and plantar flexor virtual actuators develop torque depending on the gait state estimate from the state machine.

The transition to swing phase when the foot leaves the ground is detected by either a drop in total ankle torque to less than 5 N·m, as measured using the pyramid strain gauges, or a drop in measured ankle angle, θ, below -0.19 radians to prevent angle sensor saturation. Positive torque is defined as actuator torque tending to plantar flex the ankle, and positive angles correspond to dorsiflexion. To prevent premature state transitions, the ankle torque developed during the stance phase must exceed 20 N·m for these transitions to be enabled. In addition, a 200 ms buffer time provides a minimum time frame for the stance period. The transition to stance phase upon heel-strike is detected by a decrease in torque below -7 N·m as measured using the pyramid strain gauges.

2) Dorsiflexor Model: The dorsiflexor in Fig. 5(a) is the dorsiflexor actuator. It represents the Tibialis Anterior and other biological dorsiflexor muscles. This dorsiflexor is implemented as a virtual rotary spring-damper with a set point of $[\theta = 0, \dot{\theta} = 0]$ and relation

$$\mathrm{T}_{\mathrm{dorsi}} = K_P\theta + K_V\dot{\theta}. \tag{1}$$

Here, K_P is the spring constant, and K_V is the damping constant, θ is the ankle angle and $\dot{\theta}$ is the ankle angular velocity. For the stance phase, the value of K_P was optimized along with other muscle model parameters to best match the stance phase

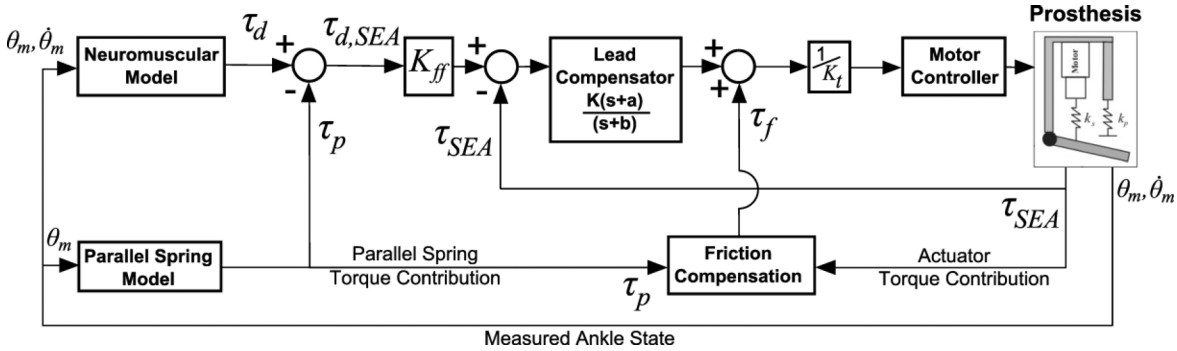

Fig. 3. Control system block diagram. The prosthesis measured ankle state, $(\theta_m, \dot{\theta}_m)$ is used to produce a torque command from the neuromuscular model, τ_d. This desired ankle torque is fed through a torque control system to obtain a current command to the prosthesis actuator. The three primary components of this torque control system are the feedforward gain $K_{\rm ff}$, lead compensator, and friction compensation term. The parallel spring contribution to prosthesis ankle torque, τ_p, is subtracted from the desired ankle torque to obtain the desired actuator torque $\tau_{\rm d,SEA}$. The closed-loop torque controller then enforces the desired actuator torque using the measured actuator torque, $\tau_{\rm SEA}$. Finally, the friction compensation term produces an additional torque value, τ_f, which is added to the output of the closed-loop torque controller.

behavior of the biological ankle for normal level-ground walking. The damping term, K_V, was experimentally tuned for stance phase to 5 Nm-s/rad to prevent the forefoot from bouncing off the ground at foot-flat. Also during the stance phase, the dorsiflexor acts only to provide dorsiflexion torque, so to mimic the unidirectional property of biological muscles. Furthermore, when the torque generated by the dorsiflexor drops to zero during stance as a result of the foot becoming perpendicular to the shank, the dorsiflexor is disabled for the remainder of the stance phase. Therefore, the dorsiflexor only contributes to the torque production early in the stance phase, when human dorsiflexor muscles are known to play a significant role [32]. In the swing phase, the dorsiflexor acts as a position controller, driving the foot to the set-point $[\theta = 0, \dot{\theta} = 0]$. For this, a gain of $K_P = 220$ N·m/rad and damping constant of $K_V = 7$ N·m·s/rad provides for quick ground clearance of the foot early in the swing phase.

3) Plantar Flexor Model: The virtual plantar flexor in Fig. 5 comprises a muscle–tendon complex, (MTC) which represents a combination of human plantar flexor muscles. The MTC is based on [28] where it is discussed in further detail. It consists of a *contractile element* (CE) which models muscle fibers and a *series element* (SE) which models a tendon. The contractile element consists of three unidirectional components: a Hill-type muscle with a positive force feedback reflex scheme, a high-limit parallel elasticity, and a low-limit, or buffer, parallel elasticity. In series with the contractile element is the series element, which is a nonlinear, unidirectional spring representing the Achilles tendon. The attachment geometry of the muscle–tendon complex to the ankle joint model is nonlinear, complicating the calculation of torques resulting from the actuator force.

a) Plantar Flexor Series Elastic Element: The series elastic element (SE) operates as a tendon in series with the muscle contractile element as in [29]. Taking ε as the tendon strain defined as

$$\varepsilon = \frac{l_{\rm SE} - l_{\rm slack}}{l_{\rm slack}} \tag{2}$$

where $l_{\rm SE}$ is the length of the series element and $l_{\rm slack}$ is its rest length, the series element is specified to be a nonlinear spring described by [29]

$$F_{\rm SE} = \begin{cases} F_{\max}\left(\varepsilon / \varepsilon_{\rm ref}\right)^2, & \varepsilon > 0 \\ 0, & \varepsilon \le 0 \end{cases} \tag{3}$$

where $F_{\max}$ is the maximum isometric force that the muscle can exert. Following [29], this quadratic form was used as an approximation of the commonly-modeled piecewise exponential-linear tendon stiffness curve. This approximation was made so to reduce the number of model parameters.

b) Plantar Flexor Contractile Element: The contractile element (CE) of the plantar flexor virtual actuator, Fig. 5(c), is a Hill-type muscle model with a positive force feedback reflex scheme. It includes active muscle fibers to generate force, and two parallel elastic components, as in [28]. The Hill-type muscle fibers exert a unidirectional force. This force is a function of the muscle fiber length, $l_{\rm CE}$, velocity, $v_{\rm CE}$, and muscle activation, A. The resulting force, $F_{\rm MF}$ is, as in [29], given by

$$F_{\rm MF}(l_{\rm CE}, v_{\rm CE}, A) = F_{\max} f_L(l_{\rm CE}) f_V(v_{\rm CE}) A. \tag{4}$$

The force-length relationship, $f_L(l_{\rm CE})$, of the Hill-type muscle is a bell-shaped curve given by

$$f_L(l_{\rm CE}) = \exp\left[c\left|\frac{l_{\rm CE} - l_{\rm opt}}{l_{\rm opt} w}\right|^3\right] \tag{5}$$

where $l_{\rm opt}$ is the contractile element length, $l_{\rm CE}$, at which the muscle can provide the maximum isometric force, $F_{\max}$. The parameter w is the width of the bell-shaped curve, and the parameter c describes the curve's magnitude near the extremes of the bell, where

$$f_L(l_{\rm CE} = (1 \pm w) l_{\rm opt}) = \exp(c). \tag{6}$$

The force-velocity relationship, $f_V(v_{\rm CE})$, of the CE is the Hill equation

$$f_V(v_{\rm CE}) = \begin{cases} (v_{\max} - v_{\rm CE})/(v_{\max} + K v_{\rm CE}), & v_{\rm CE} < 0 \\ N + (N-1)\dfrac{v_{\max} + v_{\rm CE}}{7.56 K v_{\rm CE} - v_{\max}}, & v_{\rm CE} \ge 0 \end{cases} \tag{7}$$

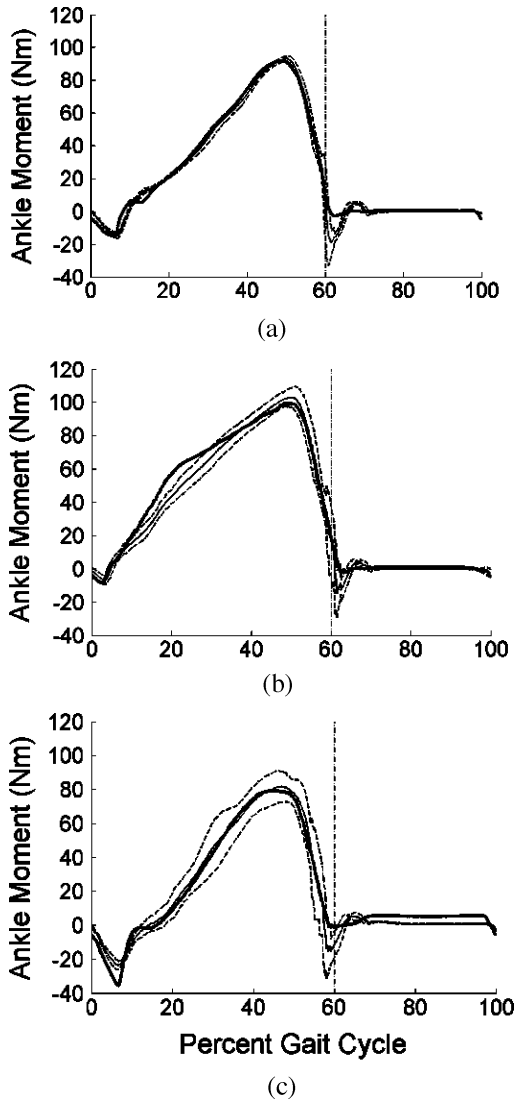

Fig. 4. Prosthesis torque tracking over one complete gait cycle (heel-strike to heel-strike of the same foot) for three walking conditions: (a) level-ground, (b) ramp ascent, and (c) ramp descent. Shown are commanded torque mean ± standard deviation (thin line), and prosthesis torque, as estimated using the measured SEA torque contribution and angle-based estimate of the parallel spring torque contribution (thick line). The vertical (dashed–dot) line indicates the end of the stance phase.

where $v_{\max} < 0$ is the maximum contractile velocity of the muscle, $v_{\rm CE}$ is the fiber contraction velocity, K is the curvature constant, and N defines the dimensionless muscle force (normalized by $F_{\max}$) such that

$$N = f_V(v_{\rm CE} = -v_{\max}). \tag{8}$$

Following [28], the force-length relationship for the high-limit parallel elasticity (HPE), set in parallel with the CE, is given by

$$F_{\rm HPE}(l_{\rm CE}) = \begin{cases} F_{\max}[(l_{\rm CE} - l_{\rm opt})/(l_{\rm opt}w)]^2, & l_{\rm CE} > l_{\rm opt} \\ 0, & \text{otherwise.} \end{cases} \tag{9}$$

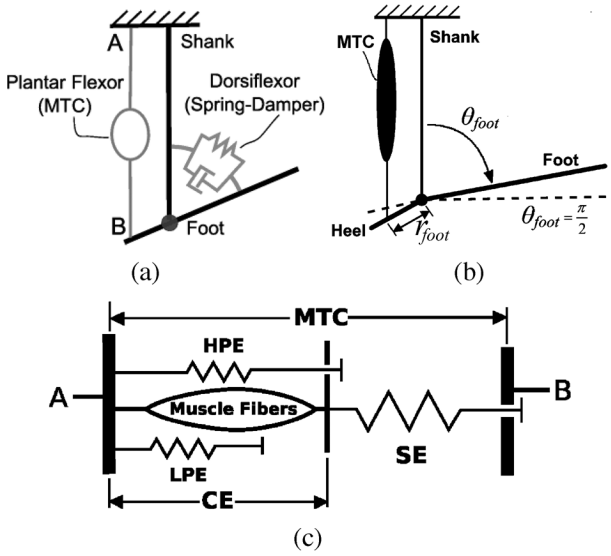

Fig. 5. Musculoskeletal model as implemented on the prosthetic microcontroller, including the Hill-type muscle model and spring-damper attachments to the two-link ankle joint model (a), geometry of the muscle model skeletal attachment including the variable moment-arm implementation and angle coordinate frame for the muscle model (b), and detailed Hill-type muscle model (c).

A low-limit, buffer parallel elasticity (LPE) is also included, based on [28]. This was given the form of the nonlinear spring

$$F_{\rm LPE}(l_{\rm CE}) = \begin{cases} F_{\max}\dfrac{[(l_{\rm CE} - l_{\rm opt}(1-w))/l_{\rm opt}]^2}{(w/2)}, & l_{\rm CE} \le l_{\rm opt}(1-w). \\ 0, & \text{otherwise.} \end{cases} \tag{10}$$

Therefore, the total plantar flexor force is described by

$$F_{\rm CE} = F_{\rm MF}(l_{\rm CE}, v_{\rm CE}, A) + F_{\rm HPE} - F_{\rm LPE} \tag{11}$$

where $F_{\rm CE}$ is the force developed by the contractile element. Since the CE and SE are in series, the following equation holds: $F_{\rm CE} = F_{\rm SE} = F_{\rm MTC}$.

c) Reflex Scheme: The contractile element activation, A, is generated using the positive-force feedback reflex scheme shown in Fig. 6, as in [28], [29]. This feedback loop includes a stance phase switch for disabling the plantar flexor force development during the swing phase. During stance, the plantar flexor force, $F_{\rm MTC}$, is multiplied by a reflex gain $\text{Gain}_{\rm RF}$, delayed by $\text{Delay}_{\rm RF}$ and added to an offset stimulation, *PRESTIM* to obtain the neural stimulation signal. The stimulation is constrained to range from 0 to 1, and is low-pass filtered with time constant T to simulate the muscle excitation-contraction coupling. The resulting signal is used as activation in (4) with an initial value of *PreA*. In addition, a suppression gain, $\text{Gain}_{\rm SUPP}$, following [28], was implemented to help prevent the two actuators from fighting each other during stance. Here, the torque generated by the dorsiflexor is reduced by either $\text{Gain}_{\rm SUPP} \cdot F_{\rm MTC}$ or until its value drops to zero.

d) Plantar Flexor Geometry and Implementation: Within the muscle model framework, the ankle angle, $\theta_{\rm foot}$, is defined as shown in Fig. 5(b). Using this angle as the input to the model,

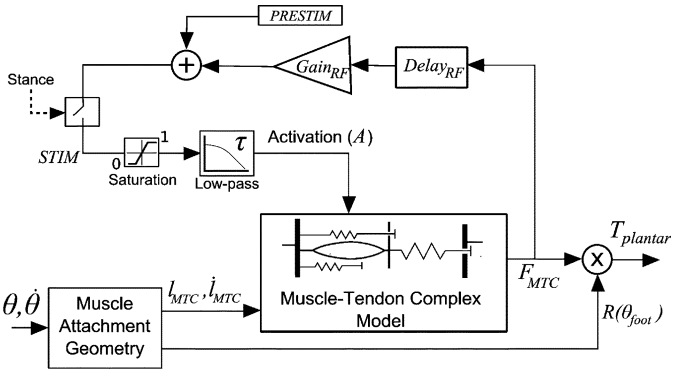

Fig. 6. Reflex scheme for the virtual plantar flexor muscle, including the relationship among ankle angle, muscle force, and the plantar flexor component of ankle torque.

the length of the muscle–tendon complex is calculated as in [28] by

$$l_{\mathrm{MTC}} = r_{\mathrm{foot}}\rho(\sin(\phi_{\mathrm{ref}} - \phi_{\max}) - \sin(\theta_{\mathrm{foot}} - \phi_{\max})) + l_{\mathrm{slack}} + l_{\mathrm{opt}} \quad (12)$$

where ρ is a scaling factor representing the pennation angle of the muscle fibers, and ϕ_{ref} is the ankle angle at which $l_{\mathrm{CE}} = l_{\mathrm{opt}}$ under no load.

The fiber length, l_{CE} can be computed using $l_{\mathrm{CE}} = l_{\mathrm{MTC}} - l_{\mathrm{SE}}$, where l_{SE} is obtained from the inverse of (3) given the current value of $F_{\mathrm{CE}} = F_{\mathrm{SE}} = F_{\mathrm{MTC}}$ from the muscle dynamics. The fiber contraction velocity, v_{CE}, can then be obtained via differentiation. This creates a first order differential equation governed by the dynamics of the neuromuscular model. This equation can be solved for F_{MTC} given the time history of θ_{foot} and initial condition. However, since integration is computationally more robust than differentiation, an integral form of this implementation was used to solve for F_{MTC}, as described in [28].

Given the attachment radius, r_{foot}, and the angle, $\phi_{\max}$, at which maximum muscle–tendon moment arm is realized, the relationship between F_{MTC} and the resulting plantar flexor contribution to ankle torque, T_{plantar}, is given by

$$\begin{aligned} T_{\mathrm{plantar}} &= F_{\mathrm{MTC}} \cos(\theta_{\mathrm{foot}} - \phi_{\max}) r_{\mathrm{foot}} \\ &= F_{\mathrm{MTC}} \cdot R(\theta_{\mathrm{foot}}) \end{aligned} \quad (13)$$

where $R(\theta_{\mathrm{foot}})$ is a variable moment arm resulting from the muscle attachment to the ankle joint model. This relationship is shown graphically in Fig. 6. Hence, the plantar flexor model can ultimately be treated as a dynamical system linking a single input, θ_{foot}, to a single output, T_{plantar}.

4) Neuromuscular Model Parameter Determination: The plantar flexor model is a lumped representation of all of the biological plantar flexor muscles. Likewise, the dorsiflexor represents all biological dorsiflexor muscles. In this work, joint and torque measurements were taken only at the ankle joint. As a result, the state of multi-articular muscles, such as the gastrocnemius, could not be accurately estimated. Therefore the plantar flexor was based upon the dominant monarticular plantar flexor in humans, the Soleus. The majority of the plantar flexor parameters values are those reported in [28] for the Soleus muscle, as shown in Table I. Some parameters of the plantar flexor, as well as those for the dorsiflexor, however, were expected to either have been significantly affected by the lumped models, or were not well known from biology. These six parameters were fitted using a combination of a Genetic Algorithm and gradient descent to enable the neuromuscular model to best match the walking data of an intact subject.

TABLE I
NONOPTIMIZED PARAMETER VALUES

Parameter (Units)	Value	Parameter (Units)	Value
l_{opt} (m)	0.04	w	0.56
l_{slack} (m)	0.26	c	ln(0.05)
v_{max} (l_{opt}/s)	6.0	N	1.5
ε_{ref}	0.04	K	5
$PreA$	0.01	ρ	0.5
T (s)	0.01	r_{foot} (m)	0.05
$PreSTIM$	0.01	$Delay_{RF}$ (s)	0.02

a) Non-Amputee Subject Data Collection: Kinetic and kinematic walking data were collected at the Gait Laboratory of Spaulding Rehabilitation Hospital, Harvard Medical School, in a study approved by the Spaulding committee on the Use of Humans as Experimental Subjects [33]. A healthy adult male (81.9 kg) was asked to walk at slow walking speed across a 10 m walkway in the motion capture laboratory after informed consent was given.

The motion-capture was performed using a VICON 512 motion-capture system with eight infrared cameras. Reflective markers were placed at 33 locations on the subject's body in order to allow the infrared cameras to track said locations during the trials. The cameras were operated at 120 Hz and were able to track a given marker to within approximately 1 mm. The markers were placed at the following bony landmarks for tracking the lower body: bilateral anterior superior iliac spines, posterior superior iliac spines, lateral femoral condyles, lateral malleoli, forefeet, and heels. Wands were placed over the tibia and femur, and markers were attached to the wands over the mid-shaft of the tibia and the mid-femur. Markers were also placed on the upper body at the following sites: sternum, clavicle, C7 and T10 vertebrae, head, and bilaterally on the shoulder, elbow, and wrist joints.

Ground reaction forces were measured using two staggered force plates (model no. 2222 or OR6-5-1, by Advanced Mechanical Technology Inc., Watertown, MA) which were incorporated into the walkway. The precision of these force plates measuring ground reaction force and center of pressure is approximately 0.1 N and 2 mm, respectively. The force plate data was collected at 1080 Hz and synchronized with the VICON motion capture data. Joint torques were calculated from the ground reaction forces and joint kinematics using a modified version of a standard inverse dynamics model. Vicon Bodybuilder (Oxford Metrics, Oxford, U.K.) was used to perform the inverse dynamics calculations.

Six trials were obtained for a slow level-ground walking speed (1.0 m/s mean) and a single trial was used to represent the target ankle and torque trajectories for this walking condition. The end of the stance phase was defined as the point in time when the joint torque first dropped to zero after the peak torque

TABLE II
OPTIMIZATION PARAMETER RANGES

Parameter (Units)	Minimum Value	Maximum Value
F_{max} (N)	3000	7000
$Gain_{FB}$	0.6	1.5
K_P (N·m/rad)	20	250
$Gain_{SUPP}$	0	5
ϕ_{ref} (rad)	0.52	2.09
ϕ_{max} (rad)	1.40	2.44

TABLE III
FITTED VALUES OF NEUROMUSCULAR MODEL PARAMETERS

Parameter (Units)	Value
F_{max} (N)	3377
$Gain_{FB}$	1.22
K_P (N·m/rad)	72.9
$Gain_{SUPP}$	0
ϕ_{ref} (rad)	1.49
ϕ_{max} (rad)	1.95

was reached in the gait cycle. This event occurred at 67% gait-cycle for the selected trial.

b) Fitting of Model Parameters to Experimental Data via Optimization: The following parameters were chosen for tuning: $F_{\max}, \mathrm{Gain}_{\mathrm{FB}}, \mathrm{Gain}_{\mathrm{SUPP}}, \phi_{\mathrm{ref}}$, and $\phi_{\max}$. The goal of the parameter tuning was to find the parameter set that would enable the neuromuscular model to best match a biological ankle torque trajectory for a particular walking condition, given the corresponding biological ankle angle trajectory as input to the model. The cost function for the optimization was defined as the squared error between the biologic and model torque profiles during the stance phase, given the biological ankle angle trajectory, i.e.,

$$\mathrm{Cost} = \sum_{t \in \mathrm{STANCE}} (T_m(t) - T_{\mathrm{bio}}(t))^2 \qquad (14)$$

where T_m is the torque output of the model, and T_{bio} is the biological ankle torque.

A Genetic Algorithm optimization was chosen to perform the initial search for optimal parameter values, and a direct search was included to pinpoint the optimal parameter set. The Genetic-Algorithm tool in Matlab was used to implement both optimization methods. The level-ground human walking data at the selected 1.0 m/s walking speed was used to provide the reference behavior for the optimization. The allowable range for each of the optimization parameters can be seen in Table II.

The initial population was chosen by the optimizer. The parameter values obtained from the parameter optimization are shown in Table III.

As a verification of the optimization effectiveness, the optimization was run with the final parameters using the biological ankle angle profile as input to the neuromuscular model. A comparison of the resulting torque profile to the biologic torque profile is shown in Fig. 8.

5) Low-Level Torque Control: The physical torque actually produced at the ankle joint during stance phase is from the combined actions of the parallel spring and the motorized drive train.

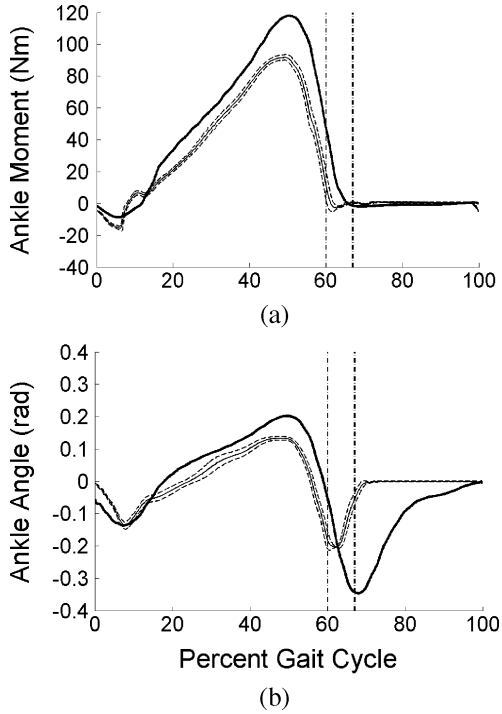

Fig. 7. Prosthesis measured torque and angle trajectories during trials with an amputee subject compared to those of the biological ankle of a weight and height-matched subject with intact limbs. Shown are ankle torque (a) and ankle angle (b) over a level-ground gait cycle from heel-strike (0% Cycle) to heel-strike of the same foot (100% Cycle). Plotted are mean ± one standard deviation for the prosthesis measured torque and angle profiles resulting from the neuromuscular-model control, (thin line) and the ankle biomechanics for a gait cycle of the weight and height-matched subject with intact limbs (thick line) at the same walking speed (1 m/s). The vertical lines indicate the average time of the beginning of swing phase for the prosthesis gait cycles (thin dashed–dot line) and the beginning of the swing phase of the biological ankle (thick dashed–dot line).

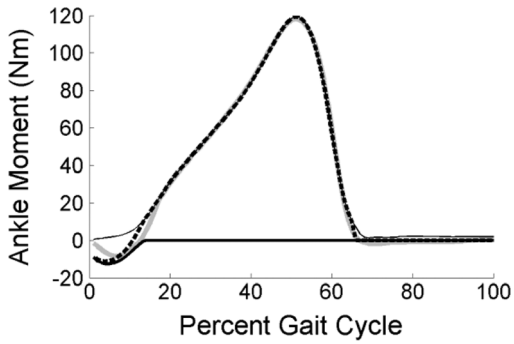

Fig. 8. Results of the parameter optimization. Shown is a comparison of the ankle moment profile from the intact biological ankle to that of the neuromuscular model with the biological ankle angle profile as the input, and with optimized parameter values. Shown are biological ankle moment (gray line), modeled dorsiflexor component (thick dark line), modeled plantar flexor muscle component (thin line), and total neuromuscular model (plantar flexor and dorsiflexor) moment (dashed line). The neuromuscular model ankle moment matches the biological ankle moment almost exactly for most of the gait cycle.

The rotary parallel spring stiffness is approximately linear in the range of operation, with a spring stiffness of 500 N·m/rad. Using this spring constant, the parallel spring contribution is predicted and subtracted from the desired ankle torque. The remaining torque must be produced by the motorized drive train.

The performance of the motorized drive train is improved by use of lead compensation, friction compensation and feedforward techniques, as shown in Fig. 3. Experimental investigations of the open loop drive train dynamics were performed and used to implement these improvements [34]. The output torque versus commanded torque for level-ground walking, ramp ascent, and ramp descent is shown in Fig. 4. The prosthesis output torque was estimated using the strain gauge on the series spring for the SEA torque contribution, and the ankle angle-based parallel spring torque estimate for the parallel spring torque contribution.

C. Clinical Evaluation

The clinical experiments were approved by MIT's Committee on the Use of Humans as Experimental Subjects (COUHES). The study participant was a volunteer and was permitted to withdraw from the study at any time and for any reason. Before taking part in the study, the participant read and signed a statement acknowledging informed consent.

The prosthesis was placed on the right leg of a healthy, active, 75 kg transtibial amputee. The subject was allowed time to walk on the prosthesis for natural adjustment. The wireless link to the prosthesis was used to record the walking data from these trials.

During the level-ground walking trials, the subject was asked to walk across a 10-m-long path. The target intended walking speed was set to 1.0 m/s to match that of the intact subject. The subject began walking approximately 5 m from the beginning of the pathway, and stopped walking approximately 3 m past the end of the path. Markers on the ground were used to note the beginning and end of the 10 m path. A stopwatch was used to verify the average walking speed for each trial by noting when the subject's center of mass passed over each of the markers. A total of 10 trials were captured. Trials with walking speeds within 5% of the target speeds were used for processing, resulting in 45 gait cycles.

The subject was next asked to walk up an 11°, 2-m-long incline at a self-selected speed. The subject started on level-ground approximately 2 m from the start of the incline and stopped approximately 1 m past the incline on a platform for 10 ramp-ascent trials. This same path was then navigated in reverse for 12 ramp-descent trials.

D. Data Analysis

The first three and last three gait cycles of the level-ground trials were assumed to be transients, and were therefore ignored. Each of the remaining gait cycles were re-sampled to span 1000 data points. Mean and standard-deviation trajectories were computed from the resulting data.

For both ramp ascent and descent, the last step on the ramp was used as the representative gait cycle. Each selected gait cycle was re-sampled and averaged in the same manner as described for the level-ground trials.

The net work was calculated for each individual gait cycle by numerically integrating ankle torque over ankle angle from heel-strike to toe-off. Here the swing phase was ignored for the network calculations. The average net work for each walking condition was then computed from the individual gait cycle net work values.

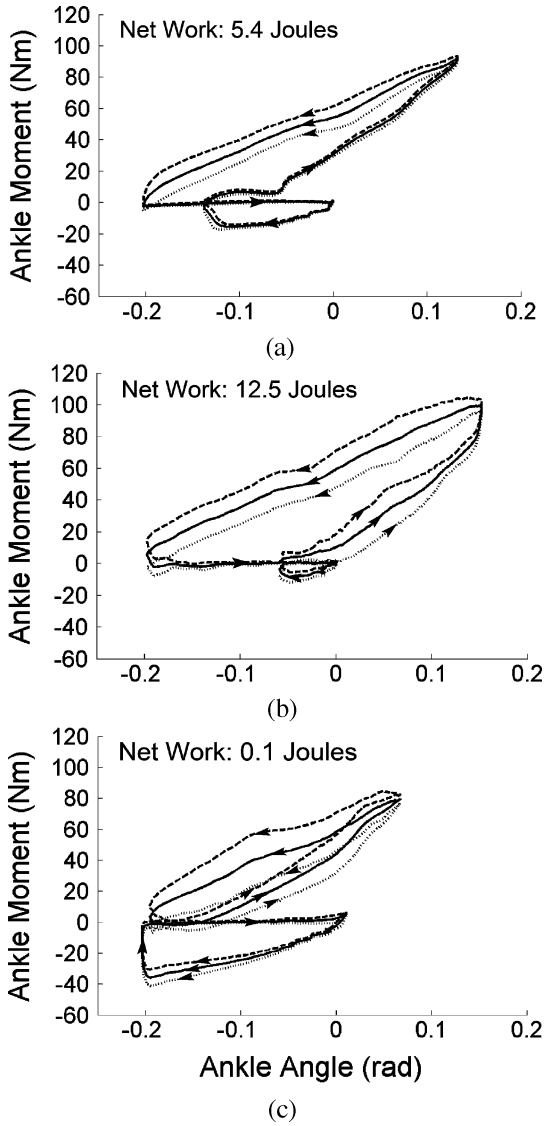

Fig. 9. Measured prosthesis torque-angle trajectories for three different walking conditions: (a) level ground, (b) ramp ascent, and (c) ramp descent. Shown are mean ± one standard deviation. Arrows indicate forward propagation in time. The average prosthesis net work increases with increasing ground slope. This result is consistent with human ankle data from the literature [35].

III. Results

A. Torque Tracking

A precondition of the present experiments was the ability of the ankle–foot prosthesis to actually produce the torques and speeds that would be commanded by the neuromuscular controller. This ability is demonstrated in Fig. 4(a)–(c), illustrating commanded torque versus measured output torque for level-ground walking, ramp ascent, and ramp descent.

B. Adaptation to Ground Slope

The evaluation of ground slope adaptation of the neuromuscular-model controlled prosthesis was confirmed by the clinical trial data of Fig. 9(a)–(c). The numerically integrated data of those trials gave net work values (work loop areas) as follows:

Level-Ground 5.4 ± 0.5 Joules
Ramp Ascent 12.5 ± 0.6 Joules
Ramp Descent 0.1 ± 1.7 Joules

C. Comparison to a Biological Ankle

The purpose of this neuromuscular model is to represent the inherent dynamics of the human ankle–foot complex in a useful way. Therefore, one may evaluate the resulting prosthesis controller based upon its ability to mimic the human behavior. Fig. 7 shows the level-ground walking torque and angle profiles from the prosthesis along with those of a weight and height-matched subject with intact limbs.

IV. Discussion

Adaptation to terrain is an important aspect of walking. However, passive ankle–foot prostheses cannot provide this ability. Even the Össur Proprio active ankle prosthesis [1] is only able to reconfigure its ankle joint angle during the swing phase, requiring several strides to converge to a terrain-appropriate ankle position at first ground contact. Further, the Proprio does not provide any of the stance phase power necessary for normal gait, and therefore cannot adapt net stance work with terrain slope. Also, the previous control methodologies of the prototype powered ankle–foot prostheses used in this study did not adapt to terrain variations owing to the significant difficulty of sensing these variations before they are encountered [24]–[26]. By contrast, the neuromuscular control presented here exhibits an inherent adaptation to ground slope without explicit sensing of terrain variation.

A. Comparable Performance to a Biological Ankle

Looking at Fig. 7, the measured ankle torque and ankle angle profiles of the prosthesis qualitatively match those of a comparable intact individual for level-ground walking. The differences observed are of a low order, and may reasonably be attributed to a number of factors, including atrophy and/or hypertrophy in the clinical subject's leg muscles resulting from amputation, differences in limb lengths, and perhaps the lack of a functional biarticular gastrocnemius muscle. In addition, the limited range of the prosthetic angle sensor prohibited the prosthesis from reaching the full range of motion of the intact ankle.

B. Ground Slope Adaptation

The increased ankle net work during ramp ascent, and the decreased ankle net work during ramp descent, as compared to that of level ground walking, is consistent with the behavior of an intact human ankle under the same conditions, according to data from [35]. This variation of stance-phase positive net work across walking conditions indicates a slope-adaptive behavior that is emergent of the neuromuscular model. The ability of the neuromuscular model to produce these biomimetic changes in behavior suggests that the model embodies an important characteristic of the human plantar flexor muscles. In addition, it is anticipated that the model has the potential for speed adaptation. In an attempt to move faster, the wearer may push harder on the prosthesis. This additional force could cause the modeled reflex to command higher virtual muscle forces, resulting in greater energy output, and hence higher walking speeds. Further investigation is needed to confirm the viability of the model for this speed-adaptive capability.

References

[1] Flex-Foot. Ossur [Online]. Available: http://www.ossur.com/?PageID=3561

[2] S. Ron, *Prosthetics and Orthotics: Lower Limb and Spinal*. Philadelphia, PA: Lippincott Williams & Wilkins, 2002.

[3] A. L. Hof, B. A. Geelen, and J. Van Den Berg, "Calf muscle moment, work and efficiency in level walking; role of series elasticity," *J. Biomechan.*, vol. 16, no. 7, pp. 523–537, 1983.

[4] D. A. Winter, "Biomechanical motor pattern in normal walking," *J. Motor Behavior*, vol. 15, no. 4, pp. 302–330, 1983.

[5] M. Palmer, "Sagittal plane characterization of normal human ankle function across a range of walking gait speeds," M.S. thesis, Massachusetts Inst. Technol., Cambridge, MA, 2002.

[6] D. H. Gates, "Characterizing ankle function during stair ascent, descent, and level walking for ankle prosthesis and orthosis design," M.S. thesis, Boston Univ., Boston, MA, 2004.

[7] A. H. Hansen, D. S. Childress, S. C. Miff, S. A. Gard, and K. P. Mesplay, "The human ankle during walking: Implication for the design of biomimetic ankle prosthesis," *J. Biomechan.*, vol. 37, no. 10, pp. 1467–1474, 2004.

[8] D. A. Winter and S. E. Sienko, "Biomechanics of below-knee amputee gait," *J. Biomechan.*, vol. 21, pp. 361–367, 1988.

[9] H. B. Skinner and D. J. Effeney, "Gait analysis in amputees," *Am. J. Phys. Med.*, vol. 64, pp. 82–89, 1985.

[10] H. Bateni and S. Olney, "Kinematic and kinetic variations of below-knee amputee gait," *J. Prosthetics Orthotics*, vol. 14, no. 1, pp. 2–13, 2002.

[11] N. H. Molen, "Energy/speed relation of below-knee amputees walking on motor-driven treadmill," *Int. Z. Angew., Physio.*, vol. 31, p. 173, 1973.

[12] G. R. Colborne, S. Naumann, P. E. Longmuir, and D. Berbrayer, "Analysis of mechanical and metabolic factors in the gait of congenital below knee amputees," *Am. J. Phys. Med. Rehabil.*, vol. 92, pp. 272–278, 1992.

[13] R. L. Waters, J. Perry, D. Antonelli, and H. Hislop, "Energy cost of walking amputees: The influence of level of amputation," *J. Bone Joint Surg. Am.*, vol. 58, no. 1, p. 4246, 1976.

[14] E. G. Gonzalez, P. J. Corcoran, and L. R. Rodolfo, "Energy expenditure in B/K amputees: Correlation with stump length," *Archs. Phys. Med. Rehabil.*, vol. 55, pp. 111–119, 1974.

[15] D. J. Sanderson and P. E. Martin, "Lower extremity kinematic and kinetic adaptations in unilateral below-knee amputees during walking," *Gait Posture*, vol. 6, pp. 126–136, 1997.

[16] A. Esquenazi and R. DiGiacomo, "Rehabilitation after amputation," *J. Am. Podiatr. Med. Assoc.*, vol. 91, no. 1, pp. 13–22, 2001.

[17] A. D. Kuo, "Energetics of actively powered locomotion using the simplest walking model," *J. Biomech. Eng.*, vol. 124, pp. 113–120, 2002.

[18] A. D. Kuo, J. M. Donelan, and A. Ruina, "Energetic consequences of walking like an inverted pendulum: Step-to-step transitions," *Exercise Sport Sci. Rev.*, vol. 33, no. 2, pp. 88–97, 2005.

[19] A. Ruina, J. E. Bertram, and M. Srinivasan, "A collisional model of the energetic cost of support work qualitatively explains leg sequencing in walking and galloping, pseudo-elastic leg behavior in running and the walk-to-run transition.," *J. Theor. Biol.*, vol. 237, no. 2, pp. 170–192, 2005.

[20] S. Au and H. Herr, "Initial experimental study on dynamic interaction between an amputee and a powered ankle-foot prosthesis," presented at the Workshop on Dynamic Walking: Mechanics and Control of Human and Robot Locomotion, Ann Arbor, MI, May 2006.

[21] S. K. Au, J. Weber, and H. Herr, "Biomechanical design of a powered ankle-foot prosthesis," in *Proc. IEEE Int. Conf. Rehabil. Robotics*, Noordwijk, The Netherlands, Jun. 2007, pp. 298–303.

[22] S. Au, J. Weber, E. Martinez-Villapando, and H. Herr, "Powered ankle-foot prosthesis for the improvement of amputee ambulation," in *IEEE Eng. Med. Biol. Int. Conf.*, Lyon, France, Aug. 23–26, 2007, pp. 3020–3026.

[23] H. Herr, J. Weber, and S. Au, "Powered ankle-foot prosthesis," in *Biomechanics of the Lower Limb in Health, Disease and Rehabilitation*, Manchester, U.K., Sep. 3–5, 2007, pp. 72–74.

[24] S. K. Au, "Powered ankle-foot prosthesis for the improvement of amputee walking economy," Ph.D. dissertation, Massachusetts Inst. Technol., Cambridge, MA, 2007.

[25] S. Au, J. Weber, and H. Herr, "Powered ankle-foot prosthesis improves walking metabolic economy," *IEEE Trans. Robotics*, vol. 25, no. 1, pp. 51–66, Feb. 2009.
[26] J. Hitt, R. Bellman, M. Holgate, T. Sugar, and K. Hollander, "The sparky (spring ankle with regenerative kinetics) projects: Design and analysis of a robotic transtibial prosthesis with regenerative kinetics," in *Proc. IEEE Int. Conf. Robot. Autom.*, Orlando, FL, May 2006, pp. 2939–2945.
[27] F. Sup, A. Bohara, and M. Goldfarb, "Design and control of a powered transfemoral prosthesis," *Int. J. Robotics Res.*, vol. 27, no. 2, pp. 263–273, 2008.
[28] H. Geyer and H. Herr, "A muscle-reflex model that encodes principles of legged mechanics predicts human walking dynamics and muscle activities," *IEEE Trans. Neural Syst. Rehabil. Eng.*, to be published.
[29] H. Geyer, A. Seyfarth, and R. Blickhan, "Positive force feedback in bouncing gaits?," *Proc. R Soc. Lond. B*, vol. 270, pp. 2173–2183, 2003.
[30] G. A. Pratt and M. M. Williamson, "Series elastic actuators," in *Proc. IEEE/RSJ Int. Conf. Intell. Robots Syst.*, Pittsburgh, PA, 1995, pp. 399–406.
[31] S. K. Au and H. Herr, "On the design of a powered ankle-foot prosthesis: The importance of series and parallel elasticity," *IEEE Robot. Automat. Mag.*, vol. 15, no. 3, pp. 52–59, Sep. 2008.
[32] J. Perry, *Gait Analysis: Normal and Pathological Function*. Thorofare, NJ: SLACK, 1992, ch. 4, pp. 55–57.
[33] H. Herr and M. Popovic, "Angular momentum in human walking," *J. Exp. Biol.*, vol. 211, pp. 487–481, 2008.
[34] M. Eilenberg, "A neuromuscular-model based control strategy for powered ankle-foot prostheses," M.S. thesis, Massachusetts Inst. Technol., Cambridge, MA, 2009.
[35] A. S. McIntosh, K. T. Beatty, L. N. Dwan, and D. R. Vickers, "Gait dynamics on an inclined walkway," *J. Biomechan.*, vol. 39, pp. 2491–2502, 2006.

Michael F. Eilenberg received the B.S. degrees in computer and systems engineering and mechanical engineering from Rensselaer Polytechnic Institute, Troy, NY, in 2006, and the S.M. degree in mechanical engineering, in 2009, from the Massachusetts Institute of Technology, Cambridge, where he is currently a Ph.D. candidate in the Department of Mechanical Engineering.

His research interests are in mechatronic system design and control, particularly as applied to rehabilitation and human augmentation technologies.

Hartmut Geyer received the Dipl. degree in physics and the Ph.D. degree in biomechanics from Friedrich-Schiller-University of Jena, Germany, in 2001 and 2005, respectively.

He is Assistant Professor at the Robotics Institute of Carnegie Mellon University. His research focuses on the principles of legged dynamics and control, their relation to human motor control, and resulting applications in rehabilitation robotics.

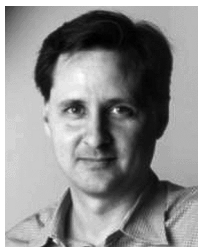

Hugh Herr (M'08) received the B.A. degree in physics from Millersville University, Millersville, PA, in 1990, the M.S. degree in mechanical engineering from the Massachusetts Institute of Technology (MIT), Cambridge, and the Ph.D. degree in biophysics from Harvard University, Cambridge, MA, in 1998.

He is Associate Professor within MIT's Program of Media Arts and Sciences, and The Harvard-MIT Division of Health Sciences and Technology. His primary research objective is to apply principles of biomechanics and neural control to guide the designs of prostheses, orthoses, and exoskeletons. He is the author of over 60 technical publications in biomechanics and wearable robotics.

Dr. Herr is the recipient of the 2007 Heinz Award for Technology, the Economy and Employment.